Full Text View

Wind-Driven Currents in the Tropical Pacific

Elise A. Ralph[*] and Pearn P. Niiler

Scripps Institution of Oceanography, La Jolla, California

ABSTRACT

An analysis is made of the ensemble mean ageostrophic near-surface circulation measured by 1503 Lagrangian drifters drogued to 15-m depth in the tropical Pacific between 1987 and 1994. It was found that the physical model of the wind-driven currents in a weakly stratified upper layer, in which the Richardson number remains near unity, accounts for 40% of the vector variance of the observations. In such a model, the amplitude of the current is proportional to $u_*(N/f)^{1/2}$ and the depth scale of the wind-driven layer is proportional to $u_*(N/f)^{-1/2}$. When the ageostrophic currents at 15-m depth are binned by the scaled Ekman depth, a net rotation of 0.87 radians was observed through the layer depth. These measurements suggest that the vertical *austausch* coefficient of the upper ocean is proportional to u_*^2/N. Ekman proposed such a model based on two reports of wind-driven currents in 1905 at widely separated latitudes.

1. Introduction

The momentum balance of large spatial scale, time-mean near-surface circulation of the ocean is between the Coriolis force, pressure gradient, and the vertical convergence of the turbulent stress due to the winds. Because this balance is linear and when the local pressure gradient is not statistically or dynamically related to the local wind (Niiler et al. 1993; Luther et al. 1990), it is in principle possible to compute local wind-driven currents from the balance of Coriolis force and the vertical convergence of the wind-produced turbulent stress, that is, the Ekman balance. The current strength depends upon the processes by which turbulence transports momentum vertically on timescales shorter than the timescale at which the Ekman balance ensues. In theories of turbulent fluid mechanics this has been a problem of considerable interest since the time of Ekman (1905). However, observations that can be used to test these theories are difficult to obtain in the open ocean because of the ubiquitous surface and internal waves. In addition, near inertial and mesoscale motions are of considerable

strength and persistence and tend to destroy the Ekman balance.

Direct measurements of vertical profiles of upper-ocean currents at single point moorings have been used to describe this Ekman balance in several important ways. Davis et al. (1981a) found that over a several week period near OWS-P, the subinertial period currents, relative to the current below the mixed layer, were statistically well correlated to the local winds. With increasing depth, the wind coherent currents rotated farther to the right of the wind. Davis et al. (1981b) were able to model the observed, vertical profile of the time-average Ekman currents in a realistic fashion with a mixed layer model in which, on near inertial and daily timescales, momentum was uniformly distributed within the mixed layer. The mixed layer deepened and became shallower according to specific partitions of turbulent energy within the mixed layer (Niiler 1975). Price et al. (1986, 1987) analyzed the structure of the daily thermocline observed near Bermuda over the summer season and demonstrated that the apparently smooth vertical spiral of velocity within this daily thermocline (again relative to a deeper current) could be modeled by a shear instability process in which, on an hourly timescale, the momentum was distributed in a uniform fashion within the mixed layer. These observations demonstrated that time-averaged Ekman spirals exist and these spirals conserve the momentum directly imparted by the wind over daily to weekly timescales, but the processes that lead to these spirals occur in the mixed layer on hourly and shorter timescales.

On longer timescales and larger space scales, measurements of the Ekman momentum balance in the upper ocean show that significant momentum is also stored beneath the equivalent time- or space-averaged mixed layer. Chereskin and Roemmich (1991) and Wijffels et al. (1994), using upper-ocean ADCP measurements averaged spatially along basinwide hydrographic sections, found that the ageostrophic, wind-driven, spiraling currents penetrated well below the spatially averaged "mixed layer," or weakly stratified layer. Chereskin (1995) found that during 90 days of persistent unidirectional summer winds over the California Current a clockwise rotating mean current relative to the 60-m current existed well below the time-average mixed layer; the Ekman balance indicated that the momentum flux from the wind was stored locally in this rotating current system. These measurements show that the mean mixed layer is not the Ekman layer and the short timescale processes that transport wind momentum vertically in the ocean can penetrate a distance comparable to the mixed layer into the well-stratified water column of the upper ocean (D'Asaro et al. 1995). Thus, the depth to which momentum is stored in the upper ocean is just as an important parameter in inferring local currents from winds as is the air–sea interaction that imparts this momentum.

The goal of this present study is to examine the relationship between the time and space ensemble-averaged 15-m depth ageostrophic currents and wind stress in the tropical Pacific. The source of the directly measured velocity is the extensive World Ocean Circulation Experiment/Tropical Oceans Global Atmosphere Surface Velocity Programme (SVP) Lagrangian drifter data (Niiler et al. 1995). The ageostrophic velocity components are computed by subtracting the historical mean 15-m geostrophic velocities from the direct measurements. The objective is also to test theories of the short time- and space-scale processes that lead to large space- and time-averaged wind-driven Ekman currents of the upper ocean. Because different theoretical assumptions about the processes that transport momentum vertically lead to different dependencies of the space–time mean current and Ekman depth on wind stress, upper-layer stratification, and Coriolis parameter, the SVP dataset that spans wide bands of latitude and air–sea interaction offers a potential for elucidation that is unique. The 15-m level current measurements cover a range of different levels of an Ekman spiral. Therefore, it is possible to resolve the spiral and fit a model of Ekman rotation and decay to the data.

2. Data

The horizontal velocities were determined from 1503 ARGOS tracked drifters deployed in the tropical Pacific between March 1987 and December 1994. A variety of different drifter configurations were used: the information on each is available from the MEDS, Canada. The great majority of the drifters were drogued to 15-m depth, and these were designed to follow water to within 1.5 cm s^{-1} in 10 m s^{-1} winds (Niiler et al. 1995). The raw ARGOS position data were processed and interpolated by krieging to 6-hourly locations at the Drifter Data Assembly Center at the Atlantic Oceanographic and Meteorological Laboratory. A five-day average velocity was computed from this data and located at the average position of the drifter during the five days. Drogues slip through the water in the direction of the wind, and the slip velocity, as determined from current meters attached to the top and the bottom of the drogue of test drifters (Niiler et al. 1995), was subtracted from the drifter velocity.

The surface wind velocity was computed from two operational products: the 6-hourly surface winds from the European Centre for Medium-Range Weather Forecasts (ECMWF) and the 6-hourly data that use the SSM/I to enhance the National Meteorological Center (NMC) products (Atlas et al. 1996). The 6-hourly wind stresses were calculated from the surface winds using a constant neutral drag coefficient of 1.2×10^{-3}. This stress and the wind were linearly interpolated spatially onto the 6-h drifter position, the slip velocity was subtracted, and both the corrected velocity and the wind stress were then averaged over 5 days, resulting in 54 600 five-day observations. These were binned into 2° latitude × 5° longitude ensembles according to the 5-day average locations and ensemble averaged. To ensure adequate sampling, boxes with less than 25 five-day measurements were eliminated from this study.

In the present study, boxes that bordered the western and eastern boundaries were eliminated. In addition, boxes within 3° of the equator were eliminated because the Ekman balance breaks down at such low latitudes (Bi 1995). We have also neglected boxes where the wind speed was less than 3 m s^{-1} because it is difficult to accurately determine the angle of the wind stress at such low wind speeds.

McPhaden et al. (1998) described the 15-m mean horizontal circulation and its variability using the drifter dataset. The time period when the greater portion of these data was acquired spans three typical seasonal cycles, the 1988 La Niña and the 1991–92–93 ENSO. Because more data was gathered during the period of persistent warming of the central tropical Pacific, the drifters' 6-yr climatology is biased toward the conditions during this warming.

In order to compute the ageostrophic 15-m velocity the surface geostrophic velocity, estimated from two hydrographic climatologies, was subtracted from the mean 15-m drifter velocities. Levitus (1982) hydrographic climatology with 1° resolution of mean temperature and mean salinity was used to compute a surface dynamic height relative to 2000 dbar. Its horizontal gradient, multiplied by g and divided by the Coriolis parameter, was used to estimate the geostrophic velocity. For comparison, Kessler (1990) provided a surface, dynamic height climatology relative to 450 m, which was enhanced by the upper-ocean XBT data and CTD data collected after 1972 and it was used to calculate the geostrophic surface currents. Taft and Kessler (1991) present a detailed comparison of geostrophic zonal currents calculated from the Kessler climatology and the Levitus climatology. These geostrophic velocities were spatially averaged into the same boxes as the drifter velocities, and the difference between the drifter velocities and the surface geostrophic velocities forms the database of the ageostrophic velocities, which are discussed here relative to the surface wind forcing. Because the dynamic topography has been smoothed to a 2° × 5° grid, the zonal geostrophic flow may be inaccurately estimated in the region of the North Equatorial Counter Current. Therefore, in this area, bounded by 10°N and 180°, all boxes with mean eastward velocity were also eliminated from the present study.

Under the fair-weather conditions that typically dominate the tropical Pacific, upper-ocean stratification is expected to play a role in the determination of the thickness and structure of the wind-driven Ekman layer. An estimate of the depth of the top of the thermocline was made from the NODC XBT dataset that spans the period from 1950 to 1990. For each cast, the distance to the top of the thermocline, D_T, was estimated as the shallowest depth at which the temperature is less than or equal to 1°C of the surface temperature. The D_T were averaged within the 2° × 5° geographical boxes. A measure of the upper-ocean stratification was taken as

$$N^2 = g\ \alpha\Delta T/(D_T\rho_o),\quad(1)$$

where α is the coefficient of thermal expansion. The mean depth D_T and the corresponding stratification are relevant parameters for estimating how deep wind mixing can penetrate without encountering a significant thermocline. However, if wind effects penetrate to this level, it is a depth from which significant amounts of heavy water must be mixed into the upper ocean. The potential energy of the water column increases at the expense of the work done by the wind or the shear ofthe currents generated by the wind in the upper ocean. The effects of rainfall in forming barrier layers (Sprintall and Tomczak 1992) and daily (or seasonal) heating (Price et al. 1986) add such important short-term constraints, and, as is demonstrated later, the scale depth of the Ekman layer determined from ageostrophic momentum balance considerations is not well correlated with D_T. The top of the thermocline D_T is also used to provide a constraint on the dataset. If D_T is less than 15 m within a 2° × 5° box, then drifters are drogued below the mixed layer and these regions must be eliminated. Five boxes in the eastern tropical Pacific were eliminated using this criterion.

3. Ageostrophic velocity

The horizontal distribution of the ageostrophic velocity relative to the wind stress shows a pattern of deflection to the right (left) of the wind stress in the Northern Hemisphere (Southern Hemisphere) (Fig. 1 ⬤▬), as is expected on a rotating earth where the Coriolis parameter changes sign across the equator. The relative strength of the ageostrophic velocity at 15-m depth compared to the wind stress is variable, as is the rotation angle. This variability of the midocean current strength and rotation will now be examined in more detail by considering a variety of models of the vertical gradient of the turbulent stress in the Ekman balance.

First, consider a model in which there is a layer H in which the turbulent stress is a linear function of depth, vanishing at its base. This is a model of Ekman balance suggested by Pollard and Millard (1970) in a study of wind-driven inertial motions in the mixed layer. A representation is sought in which the rotation angle θ relative to the wind and H are parameters to be determined by a best least square fit to the global data

$$u_a = [e^{i\theta}/H]\tau_o/\rho f.\quad(2)$$

It was found that $H = 26 \pm 3$ m and $\theta = 55° \pm 5°$. (The complex conjugates of the velocities in the Southern Hemisphere were used to fit an angle of one sign to the data.) This basin-scale rotation of the velocity relative to the wind and the depth H were independent of the climatologies of the winds and the geostrophic currents used. This model accounts for 34% of the variance in the dataset.

This slab model suggests that the stress gradient at 15-m depth is so strong that if it were uniform with depth as presumed in the strict interpretation of (2), the stress would vanish at the depth H, which is a considerable distance above the top of the main thermocline, D_T (the mean $D_T = 44 \pm 1$ m). As discussed in the introduction, observations show that the ageostrophic current penetrates to D_T. Thus, if H is interpreted as the 15-m level depth scale (Niiler and Paduan 1995), then the stress gradient must decrease significantly with increasing depth in order that the ageostrophic velocity penetrate to the top of the thermocline. In addition to the decrease of the stress-gradient, rotation of the ageostrophic current in the anticyclonic sense is expected as the depth increases from the 15-m level.

The data in Fig. 1 ⊙ shows that there is considerable spatial variability around this simple two parameter model, so it might not be the optimal model to explain the spatial variability. Consider, now, a hierarchy of models in which the depth scale for the turbulent stress, termed $H*$, can also be a function of the Coriolis parameter, wind stress, and the depth to the top of the thermocline. To examine this parameter dependence further, the amplitude of the ageostrophic current is considered first. Let

$$|u_a| = u^2_* /fH*, (3)$$

where $u^2_* = |\tau_o|/\rho$, the square of the friction velocity due to the surface stress. The goal of this paper is to determine $H*$ (and u_a) as a function of $u*$, f, and D_T with a minimal least square fit of the data to the model.

The ageostrophic velocity amplitude is modeled as

$$|u_a| = \beta u^a_* f^b D^c_T. (4)$$

The coefficient β and the exponents (a, b, c) were determined by an unbiased linear regression (Sprent 1969), which required knowledge of the errors in the estimates of the ageostrophic velocity and the model function. The errors in the model fields were estimated as the standard error of the ensemble average of measurements within each grid box; the instrumental errors were usually much smaller. The errors in the model functions were estimated by propagating the errors (using standard techniques) in $u*$, f, and D_T. The optimal values of (a, b, c) were found by determining the global minimum of the sum of the mean square differences between measured and the modeled values of the ageostrophic speed over all values of (a, b, c). The uncertainties in the exponents were found by Monte Carlo simulations. The optimal model is

$$|u_a| = (0.19)u^{1.16}_* f^{0.58} D^{-0.23}_T. (5)$$

and it accounts for 53% of the variance. The large uncertainty in c (Table 1 ⊙) suggests that the role of the mean depth of the thermocline on the ageostrophic speed was difficult to determine from this data. If c were set equal to zero in the model (4), then that optimal model, which accounts for 50% of the variance, had exponents a and b of 1.12 and −0.56, respectively, which were indistinguishable, within their uncertainties (see Table 1 ⊙), from the full model (5).

An examination of the percent of variance accounted for by the model R^2 as a function of $(a, b, 0)$ suggests that the dependence on the Coriolis parameter was better determined than the dependence on $u*$ (Fig. 2 ⊙). This result was again independent of the dynamic topography or the wind product used. The 48% curve for R^2 (95% of optimal) lies between $0.79 < a < 1.62$ and $-0.46 < b < -0.76$.

We next examined a series of dynamically constrained models that were based on physical insights of the short timescale processes that cause the vertical mixing and, thereby, set up and statistically maintain the mean Ekman layer. First, consider the model expressed in (3) in which $H* = (1/\beta)D_T$ and the amplitude coefficient β was determined from the least square fit to the data. In this model, $R^2 = 36\%$ and $\beta = 2.0 \pm 0.1$. Because β was greater than unity, the depth scale for stress was smaller than the distance to the top of the thermocline, a result which is consistent with the vector regression results discussed after Eq. (2).

The second model stems from the physical arguments of the vertical scale that is found in a nonstratified, turbulent Ekman layer, that is, $H* \propto u*/f$ (Caldwell et al. 1972). This scaling implies that near-surface currents are proportional to $u*$. This model accounted for 14% of the variance (Table 1 ⊙) in the ageostrophic speed; physically it does not represent

the parameter dependence of phenomena of daily formation and mixing of the stratified water column.

Model 3 is suggested by the austausch coefficient A_v, a large and constant turbulent viscosity coefficient parameterization of the vertical mixing. The Ekman layer depth, in this case $(A_v/2f)^{1/2}$ the amplitude of the surface current, is $u^2_*(2/fA_v)^{1/2}$. If the measurement is made at some depth z_0 (i.e., 15 m), then the scaling of the current's amplitude is a more complicated function of the parameters [in the steady Ekman solution it is $u^2_*(2/fA_v)^{1/2}\exp(-z_0(2f/A_v)^{1/2})$] and a single power law does not apply. When the Ekman scaling for the surface current was applied, the best fit determines $A_v = 2.3 \times 10^{-2}$ m^2 s^{-1}, and the model accounted for 37% of the variance (Table 1 ⊙⁼). However, the residuals between the ageostrophic velocity were negatively correlated with u_* (the correlation coefficient was −0.5). This suggested that an eddy viscosity cannot be regarded as a constant, but must be a function of u_* as well.

Ekman (1905) suggested that the "depth of frictional influence" was proportional to $u_* f^{1/2}$ and, according to the momentum balance, the amplitude of near-surface currents was proportional to $u_* f^{1/2}$ as well. This implies that the austausch coefficient A_v was proportional to u^2_*. His conclusion was based upon the reports that currents near the surface were proportional to the wind speed as reported in Mohn (1887) for the Tropics (mean latitude 9.5°) and based on the 1893–96 drift of the *Fram* (mean latitude 82°). Ekman noted that the ratio of the wind forced currents in these two reports was proportional the square root of the Coriolis parameter. His model accounted for 49% of the variance (Table 1 ⊙⁼) in our dataset of over 400 locations. When the results of all of the model speeds are plotted against the observed speed (Fig. 3 ⊙⁼) it is clear that an improvement of the scaling suggested by Ekman is evident. Ekman derived the scaling coefficient $\beta = 0.13$ compared to $\beta = 0.065 \pm 0.002$ found here based on the least squares regression across the latitute range 3° to 30°.

The steady-state scaling suggested by Ekman has a more modern interpretation in terms of the turbulent processes that transport wind momentum vertically in a weakly stratified upper ocean. Pollard et al.(1973) proposed that mixing in the upper ocean is primarily caused by the shear of near inertial motions that are caused by shifting winds and that it occurs only during those times when the Richardson number of the entire mixed layer (Ri $= N^2 H^2_*/|u_a|^2$) falls below a critical value. This constraint is equivalent to the premise that the rate of production of potential energy by entrainment at the base of the deepening mixed layer is balance by the production of turbulent mechanical energy due to the entrainment stress acting on the shear zone of the inertial motions within the mixing layer or at the base of the mixed layer. This concept, when applied to mixing of a weakly stratified column, either in bulk mixed layer models (Niiler and Krauss 1977) or in second-order closure models (Martin 1986), leads to an Ekman current scaling after the onset of a wind event of $u_* N^{1/2} f^{-1/2}$, where N is the initial stratification of the upper ocean before the event. The austausch coefficient is proportional to u^2_*/N, and the scale depth of the Ekman layer is proportional to $u_*/(fN)^{1/2}$. This scale depth, due to Pollard et al.(1973), implies that the Richardson number is $\beta^{-4}(ga\Delta T/\rho_0)$ using (1) and (4) in the definition of the Richardson number.

When N was computed from (1) and used in the regression, 51% of the variance was accounted for (Table 1 ⊙⁼). This small increase compared to Ekman's model was not surprising because $N^{1/2}$ is proportional to $D^{1/4}_T$, and the latter quantity has very small variance within the dataset. The coefficient β was equal to 0.17, which implied that the critical Richardson number for mixed layer models should be 0.77, a value consistent with what was used by Price et al.(1986) and Martin (1986) to best replicate the datasets garnered from point moorings. It is quite remarkable that the best-fit parameters for (a, b, c) in (5) were of the same sign and within the 90% confidence intervals of the physical model values of (1.0, −0.5, −0.25).

4. The Ekman spiral

The most remarkable result of the ageostrophic velocity computation was that, at every location, it was directed to the right of the wind stress in the Northern Hemisphere and to the left in the Southern Hemisphere (Fig. 1 ⊙⁼). This direction is clearly consistent with Ekman dynamics; however, there is a great deal of variability in the amount of rotation, which varies between 30° and 110°. The result of Ekman's model for steady currents or time integration of bulk mixed layers under varying winds (Davis et al. 1981b) was that the time-mean rotation within the wind-mixed layer had the same vertical scale as the vertical scale of the decrease of time mean currents with depth. It is evident from Fig. 4 ⊙ that the derived depth scale, $H_* = u_* f^{-1/2}/\beta$, varies by more than a factor of 3 over the observing domain and thus the measurements at 15-m depth should have occurred in different levels within a rotating Ekman spiral. Thus the rotation, as well as the amplitude relative to the wind, should be scaled with respect to physical scales.

There are two, possibly large, sources of uncertainties in the determination of the angle between the ageostrophic current

and the wind stress. The first was due to the uncertainty in the direction of the geostrophic currents used, which was a historical mean rather than the dynamic topography during the measurements and was spatially smoothed to fixed grids rather than to the actual scale of the phenomena. In addition there were uncertainties in the angle due to the wind products from operational products. These uncertainties, if random over the measurement domain, should average out in an ensemble that scales the amplitude and the depth scale simultaneously with respect to the scale developed in the last section.

The ageostrophic velocity data was divided into four depth bins according to the scaled vertical coordinate $z_0/H*$; each bin spans a change of 0.25 in the depth scale $z_0/H*$. The magnitude of each velocity in the bin was scaled by $\beta u* f^{-1/2}$. The rotation for vectors in the Southern Hemisphere was multiplied by -1 in order to include these measurements in the averages. It was found (Fig. 5) that the mean ageostrophic scaled velocity in the near-surface bin ($0.5 < z_0/H* < 0.75$) lay 0.85 ± 0.05 rad to the right of the wind. As $z_0/H*$ increases, the rotation with depth increases and the scaled amplitude decreases. Each 0.2 increase in $z_0/H*$ corresponds to an additional rotation of approximately 0.2 rad. The net change in the angle between the shallowest bin and the deepest bin, or through the wind driven layer, was 0.87 rad. The estimates of standard error for the bins do not overlap, indicating a statistically meaningful description of the velocity spiral has been achieved.

5. Summary and discussion

Using an ensemble-mean 15-m velocity field derived from the motion of a large number of drifting buoys in the tropical Pacific between 1988 and 1995 and removing a climatological mean geostrophic velocity, a field of ageostrophic velocity was derived. A comparison of the ageostrophic velocity with the local mean wind stress shows deflection to the right (left) in the Northern Hemisphere (Southern Hemisphere). The ageostrophic current was clearly recognizable as a current derived from almost any dynamical model of Ekman balance in which the turbulent stress decayed with depth. A series of dynamical models were fit to this data in the least square sense with the intention of identifying the physical process that leads to the development of the turbulent mixing in the subtropical Pacific.

The results of the analysis showed that the wind-driven layer on the long-term mean does not move as a uniform slab within the layer of uniform temperature. The vertical stress gradient must decrease by over 50% below the 15-m depth in order to vanish at the top of the main thermocline.

The data supports, in general, that the strongest ageostrophic currents occur in regions of strongest winds, closest to the equator. The optimum statistical model for the strength of the current as a function of wind speed, Coriolis parameter, and the mean depth of the thermocline accounted for 53% of the variance of the data and has a dependency on these parameters, which is not easily physically interpretable but does suggest a model of Richardson number limited mixing. A model of the turbulent, nonstratified Ekman layer (Caldwell et al. 1972) accounted for 14% of the variance.

A model in which the wind creates as strong a current as possible so that the Richardson number of a mixing layer in a weakly stratified upper ocean remains marginally below unity, as proposed by Pollard et al.(1973), accounts for 51% of the variance of the ageostrophic current speed. In this model, the wind-driven current strength is proportional to $u* f^{-1/2}$, and being linear in wind speed, the average current strength is also obtained from the average wind speed even though the processes that cause the vertical distribution of momentum are time-dependent and nonlinear. This scaling of the current strength implies a depth scale $u*(N/f)^{-1/2}$ that is poorly correlated (correlation coefficient 0.14) with the top of the thermocline D_T. The austausch coefficient $A_v \propto u*^2/N$ is consistent with the findings by Halpern (1974) in the upwelling zone off Oregon and Santiago-Mandijano and Firing (1990) in the central equatorial Pacific.

Further support for the relationship, $A_v \propto u*^2/N$, comes from the turbulent energy balances of the upper ocean, which have been useful in applying microstructure measurements to momentum "diffusion" in the upper ocean. The vertical turbulent viscosity in a weakly stratified water column is $A_v = u* l$. If l is the size of a typical eddy that has a velocity scale of $u*$, then dissipation ε is proportional to $u*^3/l$. The viscosity is related to the dissipation by $A_v \propto \varepsilon/N^2$. In a stratified environment the length scale l may be regarded as the buoyancy length scale $l \propto u*/N$, which all together imply that $A_v \propto u*^2/N$.

In Ekman layer theories, the vertical scale of the decay of the current strength with depth is the same as the vertical scale of the rotation of the vector with depth. Using the scale $H*$ proportional to $u* f^{-1/2}$ for the Ekman layer depth, the ageostrophic velocity data at 15 m were binned according to its level within the scaled depth. We found a posteriori that the amplitude of the currents depends on $u^2/(fH*)$; there was no exponential decay with depth. A statistically significant

Ekman spiral shows there is a rotation of a slablike velocity field throughout the upper ocean. This picture is consistent with the measurements of ageostrophic velocity in the 10°N section in the Pacific (Wijffels et al. 1994). This model of the ageostrophic velocity vector accounted for 40% of the variance in the data.

   This examination of the locally wind-driven flow relied on the assumption that the near-surface velocity field can be decomposed into a geostrophic component and a wind-driven component. For the 15-m total mean current as measured by the drifters in the tropical Pacific, 63% of the variance is accounted for by the climatological geostrophic field and 15% may be accounted for by the model of wind-driven currents in the presence of stratification. That 78% of the variance is accounted for by such a simple balance is quite heartening, considering the disparity of the datasets in time, the relatively poor sampling afforded by the hydrographic field, and the low number of drifter measurements within each box. Further work that relies of the use of the satellite sea-level variations for estimating time-dependent geostrophic currents would be valuable in understanding time-dependent models of the surface currents.

REFERENCES

Atlas, R., R. Hoffman, S. Bloom, J. Jusem, and J. Ardizzone, 1996:A multiyear global surface wind velocity dataset using SSM/I wind observations. *Bull. Amer. Meteor. Soc.,* **77,** 869–882.. Find this article online

Bi, K., 1995: Variability of the surface layer circulation in the western equatorial Pacific. Ph.D. thesis, University of California, San Diego. [Available from University of Michigan Microfilm, 305 N. Zeeb Rd., Ann Arbor, MI 48106.].

Caldwell, D., C. W. van Atta, and K. Holland, 1972: A laboratory study of the turbulent Ekman boundary layer. *Geophys. Fluid Dyn.,* **3,** 123–160..

Chereskin, T., 1995: Direct evidence for an Ekman balance in the California Current. *J. Geophys. Res.,* **100,** 18 261–18 269..

—— ,and D. Roemmich, 1991: A comparison of measured and wind-derived Ekman transports at 11°N in the Atlantic Ocean. *J. Phys. Oceanogr.,* **21,** 869–868.. Find this article online

D'Asaro, E., C. Eriksen, M. Levine, P. Niiler, C. A. Paulson, and P. V. Meurs, 1995: Upper ocean inertial currents forced by a strong storm. Part I: Data and comparison with linear theory. *J. Phys. Oceanogr.,* **25,** 2909–2936.. Find this article online

Davis, R. E., R. deSzoeke, and P. P. Niiler, 1981a: Variability in the upper ocean during MILE. I:The heat and momentum balances. *Deep-Sea Res.,* **28A,** 1427–1451..

—— ,—— ,and —— ,1981b: Variability in the upper ocean during MILE. II:Modelling the mixed layer response. *Deep-Sea Res.,* **28A,** 1453–1475..

Ekman, V. W., 1905: On the influence of the earth's rotation on ocean-currents. *Ark. Mat. Astron. Fys.,* **2,** 1–52..

Halpern, D., 1974: Observations of the deepening of the wind-mixed layer in the northeast Pacific Ocean. *J. Phys. Oceanogr.,* **4,** 459–466.. Find this article online

Kessler, W., 1990: Observations of long Rossby waves in the northern tropical Pacific. *J. Geophys. Res.,* **95,** 5183–5217..

—— ,and B. A. Taft, 1987: Dynamic heights and zonal geostrophic transports in the central tropical Pacific during 1979–1984. *J. Phys. Oceanogr.,* **17,** 97–122.. Find this article online

Levitus, S., 1982: *Climatological Atlas of the World Ocean.* NOAA Prof. Paper No. 13, U.S. Govt. Printing Office, 173 pp..

Luther, D., A. Chave, J. Filloux, and P. Spain, 1990: Evidence for local and non-local barotropic responses to atmospheric forcing during BEMPEX. *Geophys. Res. Lett.,* **17,** 949–952..

Martin, P., 1986: Testing and comparison of several mixed-layer models. Tech. Report, NORDA, 24 pp..

McPhaden, M. J., and Coauthors, 1998: The Tropical Ocean-Global Atmosphere observing system: A decade of progress. *J. Geophys Res.,* **103,** 14 169–14 240..

Mohn, H., 1887: Nordhavets Dyber, Temperatur og Stromninger: Den Norske Nordhavs-expedition 1876–1878, *II. Christiania.*..

Niiler, P., 1975: Deepening of the wind-mixed layer. *J. Mar. Res.,* **33,** 405–422..

—— , and E. Krauss, 1977: One-dimensional models of hte upper ocean. *Modelling and Prediction of the Upper Layers of the Ocean,* E. Krauss, Ed., Pergamon Press, 143–172..

—— , and J. Paduan, 1995: Wind-driven motions in the northeast Pacific as measured by Lagrangian drifters. *J. Phys. Oceanogr.,* **25,** 2819–2930.. Find this article online

—— , J. Filloux, W. Liu, R. M. Samelson, J. D. Paduan, and C. A. Paulson, 1993: Wind-forced variability of the deep eastern North Pacific: Observations of seafloor pressure and abyssal currents. *J. Geophys. Res.,* **98,** 22 589–22 602..

—— , A. S. Sybrandy, K. Bi, P. M. Poulain, and D. Bitterman, 1995:Measurements of the water-following characteristics of Tristar and Holey-sock drifters. *Deep-Sea Res.,* **42,** 1951–1964..

Pollard, R., and R. Millard, 1970: Comparison between observed and simulated wind-generated intertial oscillations. *Deep-Sea Res.,* **17,** 813–821..

—— , P. Rhines, and R. Thompson, 1973: The deepening of the wind mixed layer. *Geophys. Fluid Dyn.,* **3,** 381–404..

Price, J. F., R. A. Weller, and R. Pinkel, 1986: Diurnal cycling: Observations and models of the upper ocean response to diurnal heating, cooling and wind mixing. *J. Geophys. Res.,* **91,** 8411–8427..

—— , —— , and R. R. Schudlich, 1987: Wind-driven ocean currents and Ekman transport. *Science,* **238,** 1534–1538..

Santiago-Mandujano, F., and E. Firing, 1990: Mixed layer shear generated by wind stress in the central equatorial Pacific. *J. Phys. Oceanogr.,* **20,** 1576–1582.. Find this article online

Sprent, P., 1969: *Models in Regression and Related Topics.* Methuen, 264 pp..

Sprintall, J., and M. Tomczak, 1992: Evidence of the barrier layer in the surface layer of the Tropics. *J. Geophys. Res.,* **97,** 7305–7316..

Taft, B., and W. Kessler, 1991: Variations of zonal currents in the central tropical Pacific during 1970 to 1987: Sea level and dynamic height measurements. *J. Geophys. Res.,* **96,** 12 599–12 618..

Wijffels, S., E. Firing, and H. Bryden, 1994: Direct observations of the Ekman balance at 10°N in the Pacific. *J. Phys. Oceanogr.,* **24,** 1666–1679.. Find this article online

Wyrtki, K., 1975: Fluctuations of the dynamic topography in the Pacific Ocean. *J. Phys. Oceanogr.,* **5,** 450–459.. Find this article online
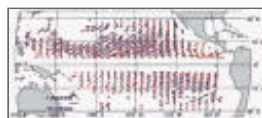

Tables

Table 1. The constants found for the linear regression models [Eq. (4)] of the magnitude of the ageostrophic velocity. The set (a,b,c) represents the exponents for the friction velocity, the Coriolis parameter, and the depth of the thermocline. The coefficient β is the amplitude coefficient of the model. See the text for a description of the seven different models.
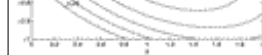

Click on thumbnail for full-sized image.

Figures

Click on thumbnail for full-sized image.

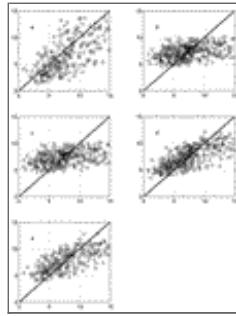Fig. 1. The mean wind stress and ageostrophic force as measured by the drifters and binned into $2° \times 5°$ boxes.

Fig. 2. A comparison of R^2, percent of variance accounted for as a function of a and b, the exponents in the model $\beta u_*^a f^b$ of the ageostrophic velocity.
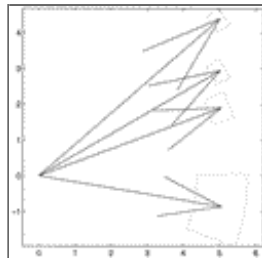
Fig. 3. Ageostrophic velocity magnitude (ordinate) vs modeled velocity (absicca). (a) Model 1: $u_*^2/(fD_T)$; (b) model 2: u_*; (c) model 3: $u_*^2 f^{-1/2}$; (d) model 4: $u_* f^{-1/2}$; and (e) model 5: $u_*/(N/f)^{1/2}$.
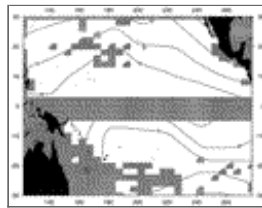
Fig. 4. The modeled Ekman depth based upon the scaling, $H_* \propto u_* f^{-1/2}$.

Fig. 5. Each arrow is the mean velocity vector within a depth range of z_0/H_*, where $H_* \propto u_* f^{-1/2}$. The amplitudes have been scaled by $\beta u_* f^{-1/2}$. The rotation to the right increases as z_0/H_* deepens. The dashed boxes around the arrowheads indicate the confidence intervals in the magnitude and rotation.

* Current affiliation: Large Lakes Observatory University of Minnesota, Duluth, Minnesota

Corresponding author address: Dr. Elise A. Ralph, Large Lakes Observatory, University of Minnesota, Duluth, MN 55812.

E-mail: llo@d.umn.edu